ISPRS Journal of Photogrammetry and Remote Sensing 78 (2013) 157–167

Contents lists available at SciVerse ScienceDirect

ISPRS Journal of Photogrammetry and Remote Sensing

journal homepage: www.elsevier.com/locate/isprsjprs

A comparison of dense matching algorithms for scaled surface reconstruction using stereo camera rigs

Ali Hosseininaveh Ahmadabadian [a,*], Stuart Robson [a], Jan Boehm [a], Mark Shortis [b], Konrad Wenzel [c], Dieter Fritsch [c]

[a] Department of Civil, Environmental and Geomatic Engineering, UCL, United Kingdom
[b] School of Mathematical and Geospatial Sciences, RMIT University, Australia
[c] Institute for Photogrammetry, University of Stuttgart, Germany

ARTICLE INFO

Article history:
Received 17 July 2012
Received in revised form 14 December 2012
Accepted 28 January 2013
Available online 8 March 2013

Keywords:
Close range photogrammetry
Structure from Motion
3D reconstruction
Multi-View Stereo
Stereo camera

ABSTRACT

Photogrammetric methods for dense 3D surface reconstruction are increasingly available to both professional and amateur users who have requirements that span a wide variety of applications. One of the key concerns in choosing an appropriate method is to understand the achievable accuracy and how choices made within the workflow can alter that outcome. In this paper we consider accuracy in two components: the ability to generate a correctly scaled 3D model; and the ability to automatically deliver a high quality data set that provides good agreement to a reference surface. The determination of scale information is particularly important, since a network of images usually only provides angle measurements and thus leads to unscaled geometry. A solution is the introduction of known distances in object space, such as base lines between camera stations or distances between control points. In order to avoid using known object distances, the method presented in this paper exploits a calibrated stereo camera utilizing the calibrated base line information from the camera pair as an observational based geometric constraint. The method provides distance information throughout the object volume by orbiting the object.

In order to test the performance of this approach, four topical surface matching methods have been investigated to determine their ability to produce accurate, dense point clouds. The methods include two versions of Semi-Global Matching as well as MicMac and Patch-based Multi-View Stereo (PMVS). These methods are implemented on a set of stereo images captured from four carefully selected objects by using (1) an off-the-shelf low cost 3D camera and (2) a pair of Nikon D700 DSLR cameras rigidly mounted in close proximity to each other. Inter-comparisons demonstrate the subtle differences between each of these permutations. The point clouds are also compared to a dataset obtained with a Nikon MMD laser scanner. Finally, the established process of achieving accurate point clouds from images and known object space distances are compared with the presented strategies.

Results from the matching demonstrate that if a good imaging network is provided, using a stereo camera and bundle adjustment with geometric constraints can effectively resolve the scale. Among the strategies for dense 3D reconstruction, using the presented method for solving the scale problem and PMVS on the images captured with two DSLR cameras resulted in a dense point cloud as accurate as the Nikon laser scanner dataset.

1. Introduction

Many methods have been presented for 3D reconstruction from one or more stereo views. Literature in this field can be divided into two general approaches: those that aim to coordinate specific features or targets on the object of interest (Godding et al., 2006) (Xiao et al., 2010) and those designed to obtain a point cloud from the object surface (Remondino and Zhang, 2006) (Grussenmeyer et al., 2009) (Fritsch et al., 2011). The first approach exploits careful design throughout to meet high accuracy industrial requirements and uses carefully designed targets, proven cameras, scale bars and an optimal image network to achieve its aims. The generality of the second approach is widely used to produce dense point clouds and textured meshes representing the form and appearance of many different surfaces. As for the target based methods, the image network configuration and definition of scale are extremely important. The success of the second approach is highly dependent

* Corresponding author.
E-mail addresses: ali.ahmadabadian.10@ucl.ac.uk (A.H. Ahmadabadian), s.robson@ucl.ac.uk (S. Robson), j.boehm@ucl.ac.uk (J. Boehm), mark.shortis@rmit.edu.au (M. Shortis), konrad.wenzel@ifp.uni-stuttgart.de (K. Wenzel), dieter.fritsch@ifp.uni-stuttgart.de (D. Fritsch).

0924-2716/$ - see front matter © 2013 International Society for Photogrammetry and Remote Sensing, Inc. (ISPRS) Published by Elsevier B.V. All rights reserved.
http://dx.doi.org/10.1016/j.isprsjprs.2013.01.015

on the quality of the imaged surface detail and the algorithms used to identify and match common detail between images. Applications and image scales are extremely varied, ranging from imaging museum artefacts to the recording of distant landforms. The relative ease with which a user base, ranging from the expert to the armchair tourist, can produce visually compelling outputs is a clear validation of the capability and robustness of the available solutions. These outcomes have raised the expectations of some of the more scientific and engineering orientated users for quantitative tools and highlight the need to narrow the accuracy gap between the industrial and the highly flexible general case.

Instead of adopting the industrial approach of independent scale bars placed in the object space, this paper reports on a strategy to combine dense point cloud generation with accurate scale based upon the calibrated distance between stereo image pairs. The known base line separation of a stereo camera allows a multitude of distances to be included as network constraints throughout, and surrounding, the object volume. Furthermore the stereo camera views help to strengthen the reliability of the starting value estimation and surface matching steps of the reconstruction process. Given a set of suitable surfaces, outputs from the developed method can be quantified through comparison against independent reference data.

A choice remains as to which reconstruction techniques to evaluate. Given common output images and orientations from bundle adjustment, the network scale constraint can be applied independently of the image matching step. Using these data it is possible to quantify the difference in performance of a variety of the image matching techniques in current use within state of the art image reconstruction solutions. The authors have selected four strategies designed to achieve a dense point cloud. Described in the following sections, they include Patch-based Multi-View Stereo (PMVS) (Furukawa and Ponce, 2009), MicMac (Pierrot-Deseilligny and Paparoditis, 2006) and two implementations of the Semi-Global-Matching (SGM) method (Hirschmüller, 2005). The first one of the two SGM implementations is using the OpenCV stereo method as described in this paper. The second implementation (Fritsch et al., 2011) is implemented close to the method as it was proposed originally by Hirschmüller, but is extended by a hierarchical approach in order to be able to process imagery with large depth variations.

2. Background

The general process of 3D reconstruction from multiple views in computer vision can be broken down into following steps (Ducke et al., 2010): feature points (key points) extraction, image matching, dense point cloud achievement, surface reconstruction and texture mapping. Examples of published work using these steps for automatic 3D modelling are given in (Beardsley et al., 1996; Pollefeys et al., 1999; Hao and Mayer, 2003; Dick et al., 2004; Nister, 2004; Agarwal et al., 2009). A growing number of software packages have also been produced including: Insight3D, Photosynth, Agisoft, Autodesk Catch 123D, and Bundler. Bundler is a well-known, open source program that determines camera parameters (interior and exterior parameters) and produces sparse 3D points incrementally. Structure from Motion (SFM) in Bundler has many steps which have been proposed over an extended period of time. As the first step, the Scale Invariant Feature Transform (SIFT) detector and descriptor are used to find keypoint locations and provide a local descriptor for each keypoint (Lowe, 1999). Next, the approximate nearest neighbour's package (Arya et al., 1998) is used to match keypoint descriptors. Within the incremental reconstruction step, an initial image pair with optimal overlap and intersection geometry is selected. The relative orientation between these two images is determined using the 5-point algorithm (Nister, 2004), followed by a bundle adjustment. Subsequently, new images are added by resecting the available 3D points using the direct linear transform (DLT) technique (Hartley and Zisserman, 2004) inside a RANSAC procedure. After the orientation of each image, a bundle adjustment is performed in order to refine the resulting orientations and 3D points. This procedure is repeated until an orientation is available for all images.

In order to extend the Bundler workflow to achieve dense point clouds, additional steps have been proposed (Seitz et al., 2006). One of the most common additions is Patch-based Multi-View Stereo (PMVS) which obtains a dense model by using the output of Bundler (Furukawa and Ponce, 2010; Ducke et al., 2010). PMVS uses undistorted images, orientation parameters of the images, a sparse set of points, and the projection matrixes to determine a dense and accurate set of rectangular patches. The implemented procedure in PMVS includes matching, expansion and filtering steps. In the matching phase, corner and blob features are found by using Harris and Difference-of-Gaussian (DoG) operators and they are matched across multiple images by taking into account local photometric consistency with Normalized Cross Correlation (NCC) to generate a sparse set of patches. Having achieved these initial matches, expansion and filtering steps are repeated three times. In the expansion step, initial matches are extended to nearby pixels to obtain a dense set of patches and in the filtering phase, incorrect matches are deleted by using visibility constraints (Furukawa and Ponce, 2009). Common to all of these methods is that a known object space distance is necessary to accurately resolve the scale for the final model (Seitz et al., 2006; Goesele et al., 2007).

The established photogrammetric 3D reconstruction procedure is typically performed as follows: design (select sensor and image network geometry), image observations and datum definition (control points, lines, coded targets and pattern recognition, inclusion of scale distances), estimating object coordinates for image observations with a robust bundle adjustment; surface reconstruction; texture mapping and visualization (Remondino and El-Hakim, 2006). These steps have been implemented in different photogrammetric packages for accurate measurement of single points (Australis, iWitness and Vision Measurement System (VMS)). In terms of 3D reconstruction, in addition to several reported attempts accomplished by photogrammetric researchers for obtaining dense and accurate point clouds from images (Remondino and Ressl, 2006; Läbe and Förstner, 2006; Roncella et al., 2005; Barazzetti et al., 2010), there are also commercial photogrammetric packages which can produce dense match output (Photomodeler Scanner, ShapeCapture and ShapeScan DSLR, VMS and iWitness). As far as the authors are aware these last solutions require either known control locations or distances in the object space to produce correctly scaled output.

The MATIS institute in Paris recently presented a new package which brings photogrammetric camera calibration methods and SFM methods together for accurate 3D reconstruction from images (Pierrot-Deseilligny and Paparoditis, 2006; Pierrot-Deseilligny et al., 2011). This package consists of Tapiaco, Apero and MicMac and supports matching point extraction with the SIFT operator, estimates interior and exterior orientation parameters based on photogrammetric strategies and finally generates a dense point cloud with a NCC stereo matching algorithm in a multi view approach. Scale can be solved by either known distances on the object space or GNSS–INS data for exterior orientation parameters.

Dense image matching is a crucial step in the reconstruction process, where correspondence information is determined for each pixel. Methodologies have been conveniently categorized into local and global (Brown et al., 2003). Local methods require a suitable choice of window size and are sensitive to locally ambiguous areas in the images (e.g. occlusion and poorly textured area). Global

methods are based on minimizing an energy function and are more robust for locally ambiguous regions, but they require significant computational effort. Semi-Global-Matching (SGM) (Hirschmüller, 2005) is a method for stereo image matching which uses an approximation of the global model to provide an efficient solution. The algorithm is widely used for various applications.

SGM is a four step method for dense image matching on stereo pairs based on a smoothness constraint global optimization of dense disparity maps. Optimisation is approximated ("*Semi*") by 1D paths through the image for efficient implementation. Beside the derivation of smooth depth maps, SGM can estimate depth without initial information about the scene. This is especially beneficial for setups, such as those used in this paper, where the relative orientation of the camera is known but no information about the actual scene is available. The four steps in the process are: pixel-wise cost computation, cost aggregation, disparity calculation and disparity refinement. The pixel-wise cost computation can be performed in different ways such as the image gradients or the squared, absolute or sampling differences of intensities in the right and left images to represent the matching quality between the two matched pixels. Cost aggregation makes a connection between costs within a certain neighbourhood. It is performed in semi-global matching by defining an energy function that depends on the disparity gradient. The aggregated cost is calculated by summing the costs of 1D minimum cost paths in all directions (minimum 4, up to 16 directions) for every pixel. The disparity computation is executed by finding the disparities which minimize the aggregated cost. Finally, disparity refinement is achieved in order to filter out peaks and noise by consistency checking and sub-pixel interpolation.

For stereo matching, the resulting disparity map contains the correspondence information for two images. Multi-View Stereo algorithms use such stereo matching methods in order to fuse their results into a network of multiple images. Beside direct solutions using the relative orientation, methods in object space are available, which optimize surfaces from overlapping range images (Zach, 2008; Merrell et al., 2007). Thus, simple stereo algorithms can be used for the benefit of speed.

3. Scale from multiple stereo camera views

3.1. Overview

A stereo camera, defined as a pair of rigidly connected cameras, is principal to this method. The camera pair should be physically stable and accurately calibrated to obtain consistent interior and relative orientation parameters. A network of stereo images is taken from successive locations as the camera pair is moved around an object. Corresponding image measurements extracted from the network are then used to compute approximate 3D coordinates which can be inserted into a bundle adjustment with the relative orientation parameters of the stereo camera as geometric constraints. If a bundle adjustment supporting such constraints is not available it is possible, but less optimal in terms of error propagation, to compare the known base line of the camera against the computed mean image pair separation and apply a suitable scale factor. After resolving the scale with one or two iterations, these data can be input into the SGM, PMVS or MicMac processing strategies to generate a dense point cloud.

3.2. Stereo camera calibration

Calibration of the stereo camera system is necessary for two reasons. First, the internal image geometric characteristics defined by physical parameters (Brown, 1971) for principal distance, principal point location, radial and decentering lens distortions, plus image affinity and orthogonally, must be estimated to remove systematic error. Second, the relative orientation of the two cameras with respect to one another must be determined simultaneously (Shortis and Harvey, 1998). Therefore, it is determined within a calibration by including an interior orientation with the internal image characteristics, a rotation of the second camera with respect to the first and a scaled translation vector. Scale is not required for a classic relative orientation, as an arbitrary value for the length of the base line vector can be adopted to obtain a solution for the remaining parameters. However for this application an accurate base length between the cameras is essential to ensure an accurate scale for the objects measured.

The image data, approximate locations and orientations of the cameras, approximate camera calibration information and initial target coordinates are then processed in the self-calibrating multi-station network solution (Granshaw, 1980). The stereo constraint can be incorporated into the network solution using a variety of different techniques (King, 1995; He et al., 1993) or the constraint can be a post-bundle computation. The network solution provides estimates and precisions of the camera calibration parameters and the locations and orientations of the cameras at each synchronised pair of exposures, enabling rigorous error propagation.

Whilst the camera calibration data are used directly in the subsequent calculations, the location and orientation data must first be transformed. The data for the many pairs of synchronised exposures are initially in the frame of reference of the calibration fixture. For VMS, each pair is transformed into a local frame of reference for the camera base line. The local frame of reference is adopted as the centre of the base line between the camera perspective centres, with the axes aligned with the base direction and the mean optical axis pointing direction. The final parameters for the relative orientation are computed as the average of the values for all synchronised pairs. Statistical analysis is used to eliminate any outliers in the stereo pairs, which are generally caused by small errors in synchronisation (Shortis and Harvey, 1998).

Estimation of the interior and relative orientation parameters of a stereo camera can be accomplished as a separate procedure before the 3D reconstruction project by capturing several convergent stereo pairs of a targeted calibration object. The procedure utilized for this paper is derived from an established single camera photogrammetric calibration solution followed by stereo pair identification and relative orientation estimation.

The calibration model adopted for this paper is equivalent to the parameter set identified by Fraser (Fraser, 1997). The parameters of this model can be reliably estimated with a self-calibrating bundle adjustment without the need for scale. However scale information can be incorporated in the relative orientation estimation. In the laboratory situation for this paper, a convergent image network design to a calibration object around which have been placed several targeted scale bars provides a practical and efficient solution. A self-calibrating bundle adjustment incorporated the camera separation between each image pair as a common geometric constraint for all image pairs taken with that camera allows simultaneous estimation of the scaled relative orientation for the camera pair.

By doing bundle adjustment using VMS as a photogrammetric bundle adjustment package, in addition to interior orientation parameters, the positions and orientations of all images are determined. In order to estimate the position and tilts of one image (right image) with respect to another (left one), a process was performed by using an extension program in VMS called Comp_RO. This program calculates the relative orientation parameters of the two images identified by three orthogonal rotations and a vector. In Comp_RO, all stereo pairs that participated in camera cali-

bration are taken into account in calculating the relative orientation, and the mean values are considered to be the positions and orientations of the stereo pair with respect to the centre of the base line and the mean pointing direction of the cameras.

3.3. Estimating initial image orientations and 3D object coordinates

The calibrated stereo camera can be effective for a wide variety of 3D reconstruction projects. For this paper, a range of geometric and freeform objects have been selected in order to highlight accuracy differences resulting from the scaling and matching strategies. All of the projects included dense orbital image networks which are ideally suited to the use of a SFM sparse reconstruction process as a network initialization tool. The most widely available SFM solution is Bundler. Although several algorithms are used in Bundler to remove outliers, the final results are not completely clean. Moreover, as special necessity for the presented method, calculating the base line in this package is not feasible. Therefore, after running this software for the images, the image observations and 3D coordinates were imported into VMS which was used for the bundle adjustment with geometric constraints to overcome the these limitations.

A program (BRS) was developed to convert Bundler output image observations and object 3D coordinates into a VMS compatible format. BRS also allowed the classification of 3D points into control and tie points based on the number of rays which exist in the bundle output for each point. The software also allowed the scaling of 3D coordinates with a defined scale factor.

3.4. Bundle adjustment with geometric constraints and scaling

Since the Bundler output is at an arbitrary scale and has a limited camera model, the subsequent application of the VMS bundle adjustment allowed not only the inclusion of the camera base line constraint on the initial data but also a full self-calibration and error propagation. To re-scale, the output inter camera separation (base line) was compared against the base line determined through laboratory calibration and the resultant scale factor used to scale the initial 3D coordinates with BRS. An iteration of the scale and VMS bundle process ensured that output coordinates were correctly scaled.

3.5. Dense point cloud generation

Given accurate exterior orientation parameters and a sparse point cloud, a robust and reliable automatic dense image matching process is needed. Exploration of widely used open and closed source implementations demonstrated that there are often several variants of established matching solutions. The following sections give specific details for each of the methods tested in this paper.

3.5.1. Pmvs

Photogrammetric exterior and interior orientation parameters of the images, and the 3D point coordinates and image observations were computed in a bundle adjustment with geometric constraints. In addition to these parameters, PMVS needs projection matrices, image observations and the sparse point cloud which were provide with the method described in (Olague and Dunn, 2007). Also, the images were undistorted following the strategy presented in (Yang et al., 2011) with camera calibration parameters extracted from bundle adjustment.

3.5.2. MicMac

In order to use MicMac for dense 3D reconstruction, Tapiaco was run on the images and the camera locations calculated by the bundle adjustment with the camera base line constraint, and then imported into Apero as GPS data. Therefore, Apero placed the camera in correct position and orientation parameters were calculated in this software by the bundle adjustment using the output of Tapiaco. Finally, a dense point cloud was generated with MicMac.

3.5.3. Semi-Global-Matching (SGM)

In order to use SGM for dense 3D reconstruction by using the interior and exterior orientation parameters from the camera base line constrained bundle adjustment, each image was undistorted and rectified with the methods presented in (Yang et al., 2011) and (Fusiello et al., 2000) respectively. After that, two versions of the SGM algorithm were applied. The first one was developed at UCL and uses the OpenCV implementation together with an approach to merge the disparity maps to support high resolution imagery. A second method was implemented by the Institute for Photogrammetry (IFP) at the University of Stuttgart. It uses a hierarchical SGM implementation for the stereo matching and a subsequent multi-base line triangulation step. In contrast to the OpenCV version, which is optimized for speed, the IFP approach is close to the original method proposed by (Hirschmuller, 2008). The key differences between the OCV SGM (UCL) method and the IFP SGM methods are given in Table 1.

A large temporary memory is needed for storing the matching costs, aggregated costs and disparity images; and the size of this memory depends on the image size and disparity range. Hirschmuller (2008) proposed a method for solving this problem by dividing the images into tiles, calculating the disparity for each tile and merging tiles into the full disparity image. Because of complexity of this method, it has not been implemented in OpenCV, thus this version of SGM can only work with low resolution images. In the first implementation of SGM (UCL version), a strategy was designed and implemented for solving this problem. Based on this strategy, images were divided into strips and disparity map was separately estimated for each strip. Within the second implementation (IFP SGM, Fritsch et al., 2011) the tiling process is used as proposed by Hirschmüller.

3.5.3.1. OCV SGM (UCL). The OpenCV implementation of the SGM method is implemented with focus on speed. Therefore, less path directions are used. Also, the pixel-wise matching cost in this version is based on the sampling insensitive measure of Birchfield and Tomasi method (Birchfield and Tomasi 1999) which can be computed more rapidly. In order to make the OpenCV version of SGM capable of working with the high resolution images for this project, instead of dividing images into tiles, images were divided into horizontal strips. The corresponding matches are almost at the same rows in the rectified images, and defining a narrow overlap area for strips is enough to obtain the proper matching without the need for either defining different disparity ranges for each strip or using disparities from low resolution images.

Given the disparity maps for the sequence of image pairs, in order to find correspondences in all images, these disparity maps were merged to each other based on geometric consistency. There are two disparity maps for almost all images in the set of images (except the first and last images) (Fig. 1). By transferring the disparity maps to the original images, two sets of image observations are produced for each of these images. The same image coordinates on these image observation sets indicate the common points for the two image pairs to which the image is belong. According to this fact, the following process was implemented in the presented method to merge the disparities: (1) transferring the disparity maps to the original images as image observation sets and (2) superimposing and merging image observation sets.

Since the final disparity maps consists of image observations in the rectified and undistorted images (not in the original images),

Table 1
Differences between the presented Semi-Global-Matching implementations.

	OCV SGM (UCL)	IFP SGM (Stuttgart University)
Path directions	8	16
Matching cost	Birchfield and Tomasi	Census or Mutual Information
Multi-image point triangulation	Tracking of points through multiple disparity images; one triangulation for all disparity images	Multiple stereo pairs for each pair; one triangulation for each image; merging in object space
Tiled processing	Yes (strips)	Yes (rectangles)
Hierarchical matching	No	Yes

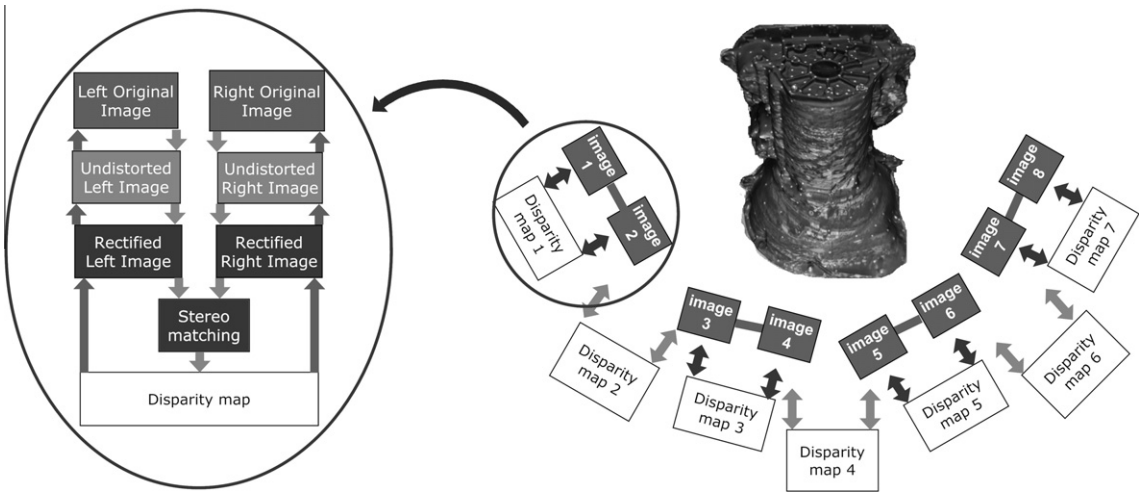

Fig. 1. The imaging network and the process of transferring disparity to the original images in the presented method.

the image observations in the disparity maps were transferred to the original images in a process with opposite transformation of producing rectified and undistorted images. Given two image observation sets for each image, these sets were overlaid. The process of overlaying was started from the right image of the first pair and it was performed for the rest of the images except the last one. Since the transferred image observations were not integer, a minimum distance (e.g. a tenth of pixel (0.1)) was chosen in order to select the common points between two image observation sets in each image and overlay them. Because each of these common points had two correspondences in the previous and next images, after the overlaying process a connection between four images was made. In order to find correspondences in all images, the common points in overlaying two image pairs were tracked in the rest of images by overlaying their image observation sets. The overlaying process was applied for image observation sets of all left images.

3.5.3.2. IFP SGM (University of Stuttgart). The IFP implementation of the SGM stereo method is close to the original method proposed by Hirschmuller (2008). In order to reduce the processing time and solve the high memory consumption problem in case of using high resolution images, a depth range was computed for each pixel individually based on the strategy mentioned in (Wenzel et al., 2011). Wenzel uses a hierarchical approach and thus enables the processing of high resolution imagery with large depth variations.

As pixel-wise matching cost, two algorithms, Census (Zabih and Woodfill, 1994) and Mutual Information (Viola et al., 1995; Hirschmüller and Scharstein, 2007), were implemented in IFP SGM. Both of these algorithms are more insensitive to radiometric changes than the Birchfield and Tomasi cost used within the OpenCV implementation. For example, a positive and a negative image could be aligned with Mutual Information (MI), because the matching cost computation is based statistically on a cross probability distribution. For the determination of this distribution, it is necessary to generate an initial disparity map which is determined in a hierarchical way. Consequently, mismatches disturb the matching cost and this makes it less robust than the Census matching cost.

An important parameter of the SGM method is the smoothness constraint, represented by penalties for disparity jumps. Large values for this penalty minimize the disparity gradients through the image which leads to smooth depth maps. In contrast, a rather low smoothness constraint is used for this investigation in order to preserve fine surface details. However, the effect of the smoothness constraint is also dependent on the matching cost, and the outcome is visible in the experimental results.

In order to extract the point clouds from the matched stereo pairs, a point triangulation step is performed for each image individually. All available disparity maps referring to this image describe corresponding image measurements. Thus, multiples of these corresponding image measurements can be used to intersect their viewing rays in object space which leads to one 3D point. This is repeated for each pixel. The high redundancy resulting from multiple disparity maps (only one stereo measurement would be required) is used to reduce the noise in the point cloud and to eliminate mismatches. Therefore, a maximum reprojection error of 0.3 pixels is applied. Furthermore, measurements with very small intersection angles (below 4°) are rejected. Subsequently, the derived point clouds are merged and thinned out in object space by keeping only the points from the cloud with the highest density for each neighbourhood. No smoothing in object space is applied.

4. Experiments and results

In order to evaluate the accuracy of 3D reconstruction, a set of reference objects were imaged with two different camera types reflecting casual and more purposed users. Firstly an off-the-shelf 3D camera (AIPTEK dual sensor camera) ($200) and secondly two

Fig. 2. From left top to right: AIPTEK dual sensor camera, our Nikon D700 stereo camera, Optoma Pico (PK301) projector, camera calibration object with Brunson scale bars; From left bottom to right: Nikon MMd laser scanner, large and small reference spheres, Nikon calibration cube and gearbox.

Nikon D700 digital SLR cameras ($4000) which were mounted base plate to base plate using a purpose manufactured adaptor. The Aiptek dual sensor camera combines the two scenes captured by a pair of lenses into a single five megapixel image (2592 × 1944 pixels). In this camera, the captured scenes of both lenses are resized in horizontal direction to store this image. Therefore, in order to have two separate images, each image is split into two parts and resized in vertical direction (two 1296 × 972 images). In comparison, each D700 camera was equipped with a 35 mm fixed focal length lens imaging onto a 12 megapixel sensor (4256 × 2832).

Both stereo cameras were calibrated with a 3D calibration fixture, equipped with 119 retro reflective targets mounted on vertical bars and a base plate (550 × 550 mm) (Fig. 2). Scale was provided by two Brunson carbon fibre scale bars equipped with retro-target tips (597.9962 ± 0.003 and 597.9904 ± 0.003 mm). A white Nikon reference cube with known inter-plane separations (inter-plane distances: 100.1660 and 95.1570) was used to validate the Nikon MMd laser scanner and also served as a test object for evaluating the accuracy of the methods. In addition to the cube, two reference spheres and a metal gearbox casting were used as test objects. Camera calibration parameters were estimated for both stereo cameras to a high level of precision (mean precision of target coordinates was 5 μm in both cases). The self-calibrations were performed with VMS which was also used to compute relative orientations of these cameras. The standard deviation of estimated base line of the AIPTEK camera was 39.953 mm (σ: 52 μm) and 102.201 mm (σ: 85 μm) for the stereo Nikon camera. Base line length uncertainties are significantly larger than the target coordinate uncertainties because of the relatively narrow angle of view of the incoming rays to each camera and the camera locations being distant from the coordinate datum.

3D surface reconstruction based on dense image matching requires varying texture on the object surface. Since all of the objects used here had little to no discernible texture, two Optoma Pico (PK301) projectors were used to project a pattern onto the surfaces. This pattern was simply chosen from pebble and gravel images to generate a fine and natural texture on the object. Strong convergent image networks (Fig. 3) were captured with each stereo camera. All images were taken with the cameras mounted on a tripod to ensure a high level of image quality. It should be noted that the 35 mm lenses fitted to the Nikon cameras and their 90° rotation provided a smaller field of view than the AIPTEK camera. Fig. 3 gives an overview of the image networks used for each object group. More images were captured with the AIPTEK camera (60 images from the gearbox and 96 images from other objects) whilst the stereo DSLR camera acquired 30 and 48 images respectively. Moreover, In terms of imaging network for the gearbox, almost all of the AIPTEK images were captured from the front of the object. Another image configuration was captured with the Nikon cameras that covered the front and sides of the gearbox casting.

Given the interior orientation parameters of the stereo cameras from self-calibration, all images were geometrically undistorted and imported into Bundler in order to automatically compute exterior orientation parameters. Bundler and the included SIFT based operator were used as they provide a highly effective automatic solution without the need for 3D control points. Bundler output data were transformed into VMS compatible format through BRS in order to compute a bundle adjustment with the camera base line constraint. This solution provided high quality exterior orientation parameter estimates and a check on object coordinate precision. The mean 3D object coordinate precision for the gearbox example was 283 μm for the AIPTEK camera and 11 μm for the stereo Nikon system. Equivalent values for the cube and sphere reference object sets were 420 μm and 32 μm respectively.

After accurately estimating exterior orientation parameters in VMS, these parameters were used in MicMac, PMVS, the modified OpenCV version of SGM and the SGM implemented at IFP, with both Mutual Information (MI) and Census matching cost, to achieve a dense point cloud for each group of images captured by both stereo cameras. The results of these methods are annotated with a star as PMVS*, MicMac*, OCV SGM*, IFP SGM* (MI), IFP SGM* (Census) in the figures and graphs. Moreover, to investigate the ability of the presented method to accurately resolve the scale, the regular process of 3D reconstruction with PMVS and MicMac was followed and the final point clouds were scaled by using known object distances. The results of these processes are shown as PMVS and MicMac without annotated star in the figures and graphs.

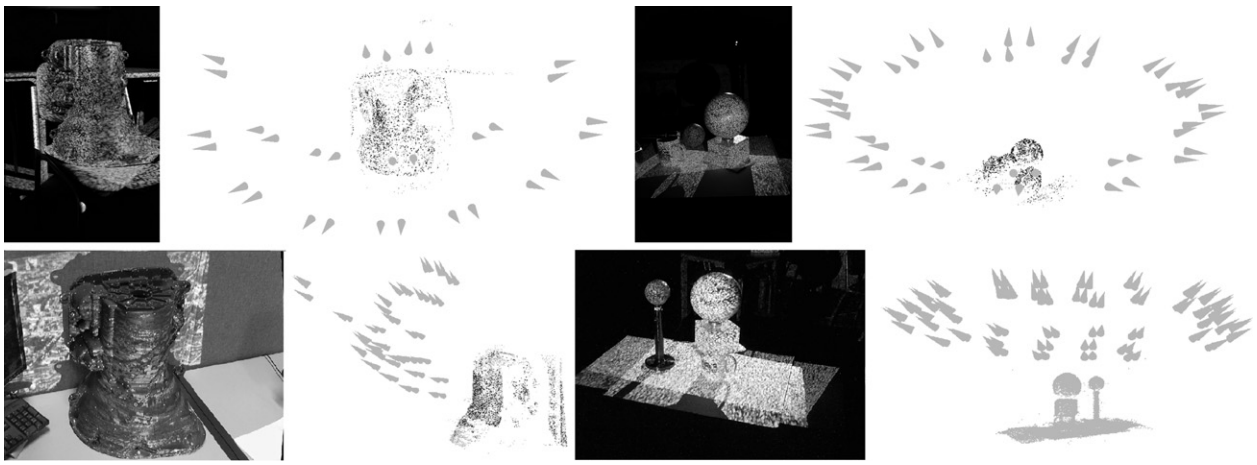

Fig. 3. example images of the textured gearbox and reference objects with Nikon stereo camera (top) and the AIPTEK camera (bottom) and the schematic imaging network for each group.

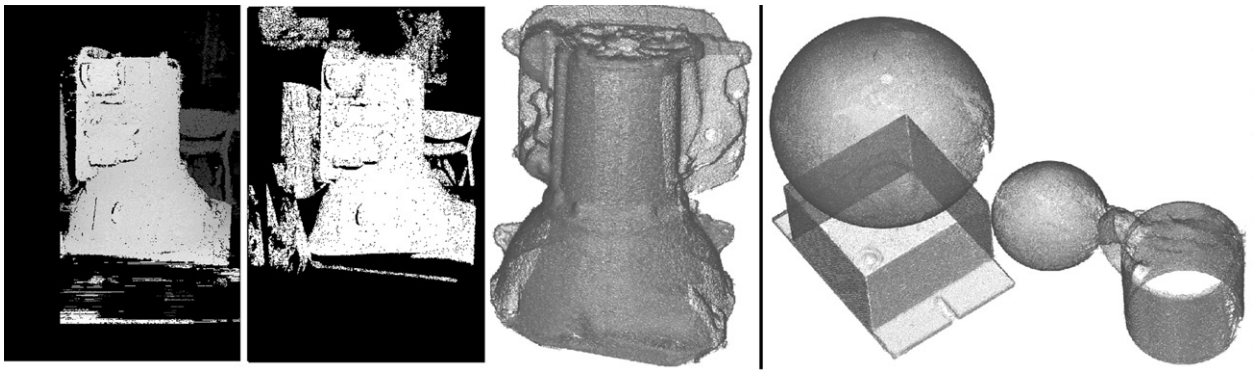

Fig. 4. Two disparity maps generated with OCV SGM* and IFP SGM* (MI), a point cloud of gearbox obtained with MicMac* and a point cloud of cube and spheres produced with PMVS*.

Fig. 4 shows disparity maps generated with OCV SGM* and IFP SGM* (MI) and two point clouds generated with the MicMac* and PMVS*. Exterior orientation parameters of the images in all of these methods were calculated with the method presented in this paper (the reason of citing the names with*). In comparison with the disparity map obtained with IFP SGM*, a black column can be seen in the left of the disparity map produced with OCV SGM*. This is due to the difference between hierarchical and direct approaches in estimating disparity for these methods. In hierarchical approach in IFP SGM*, the disparity values for high resolution images are extracted from the disparity values of low resolution images (the higher level of the image pyramid), while in the direct approach these values are calculated in the main image with a splitting strategy to overcome memory consumption problem. Thus, when a large disparity range for high resolution images is defined in the OpenCV version of SGM, a blank column appears in the left of the disparity map.

5. Comparison of the results

The accuracy of the methods for the geometric sphere and cube reference objects were evaluated based on the following quality parameters which were derived from similar parameters defined in VDI/VDE guideline (VDI/VDE 2634/Part2, 2002) (VDI/VDE 2634/Part3, 2008) using the implementation in GOM's Inspection software (GOM inspect v7 SR2).

Spherical error is defined as the range of radial distance between the measured points and a best-fit sphere and calculated according to the least squares method with a free radius for a standard sphere artefact. As can be seen in Fig. 5 (top right), the reference MMd Nikon laser scanner highlights considerable systematic error in the shape of the large sphere. This pattern was repeated in the SGM* and PMVS* results and this confirmed that the large sphere is oblate. The shape error could be a result from the manufacturing process, where two hemispheres are combined with slight pressure. This outcome is somewhat masked by the higher noise in the OCV SGM* and MicMac* datasets.

Flatness error is the range of distances between each point on the point cloud from a least squares best-fit plane. The point clouds of the cube for the methods and Nikon laser scanner were analyzed separately in this test. Fig. 6 highlights the most accurate results where PMVS* is able to produce comparable output to the laser scanner.

Fig. 7 illustrates the flatness and spherical errors of all point clouds generated with the methods from the images captured with the Nikon stereo camera and the AIPTEK stereo camera. Again PMVS* produced the highest quality point cloud in terms of flatness and spherical error. Comparing PMVS, PMVS* and also MicMac and MicMac* in this figure proves the ability of providing scale through exterior orientation directly scaled by a fixed base line, in contrast to scaling the point cloud using a ground truth technique. Although the OpenCV version of SGM was able to generate better point clouds for low resolution images than IFP SGM

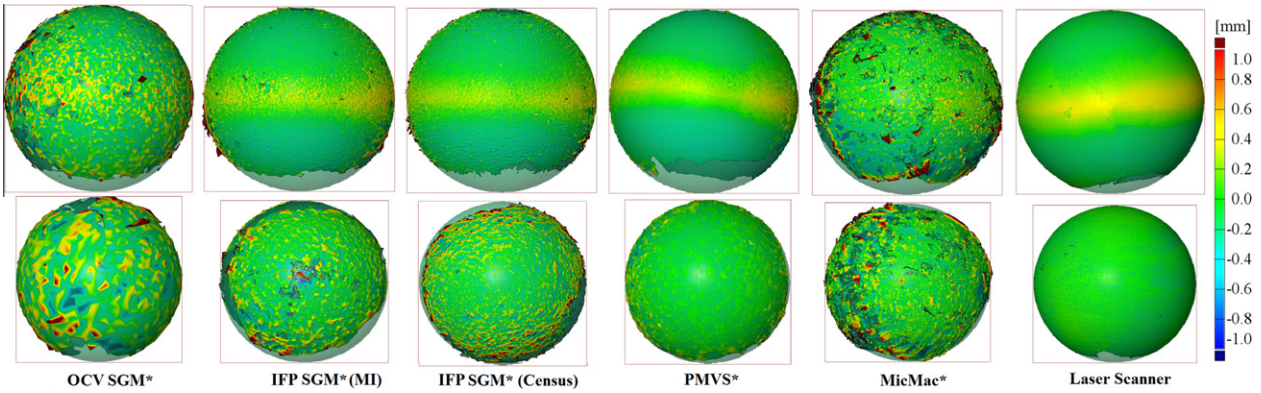

Fig. 5. Spherical errors for the presented methods implemented on the images captured with two Nikon cameras and for Nikon Laser scanner data for large (top) and small (bottom) spheres.

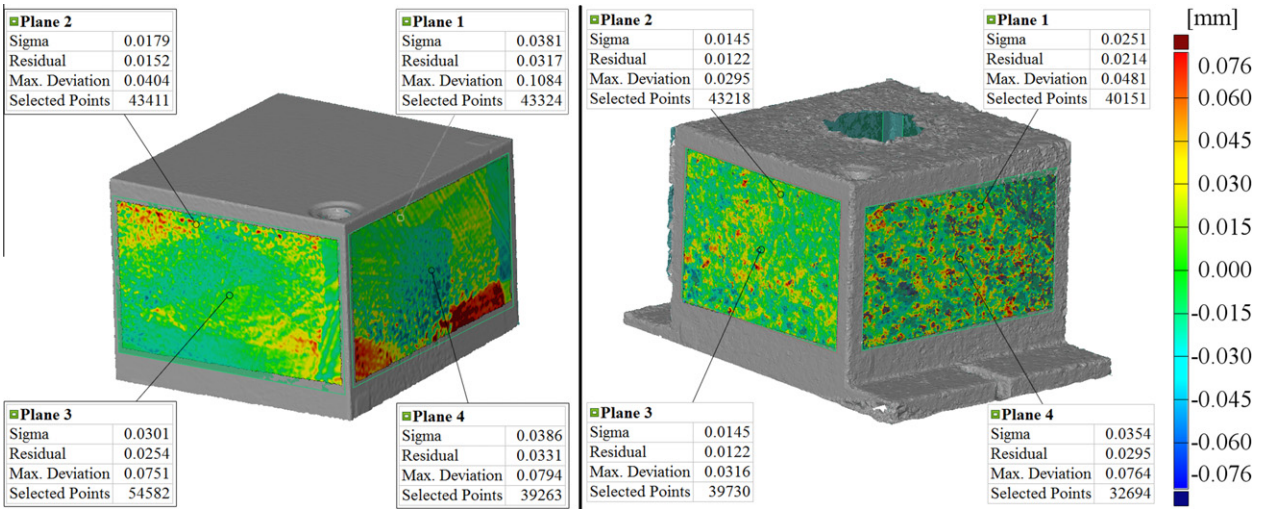

Fig. 6. Flatness error for the point cloud obtained with Nikon MMd laser scanner and PMVS*.

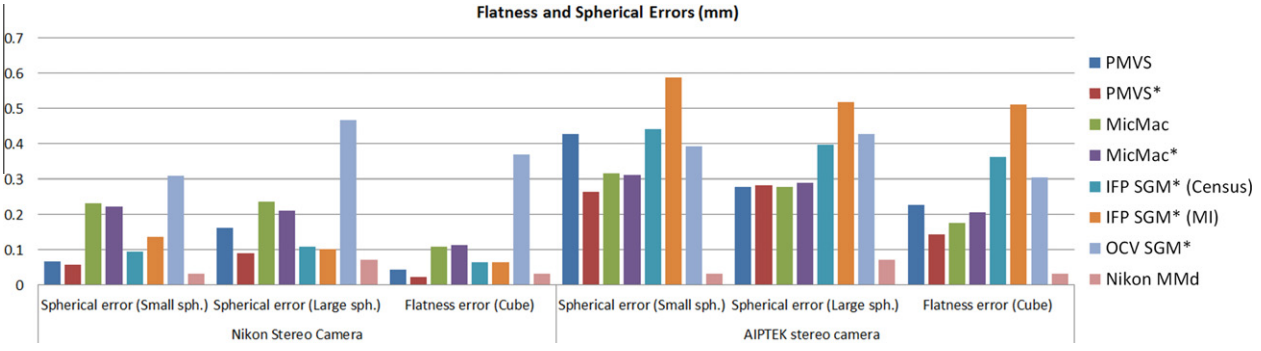

Fig. 7. Flatness and spherical error.

(MI), it was less successful in the case of the high resolution images. The reason of this behaviour can be found in the different imaging networks for the high and low resolution. In the high resolution imaging network, the spatial distance between each image pair and its next pair was too large, and thus the process of merging disparity maps in most image pairs failed even with using different thresholds for the captured area. Furthermore, the smoothness constraint of the SGM is set at a higher threshold, which is beneficial for radiometrically noisy datasets with low resolution and thus few disparity jumps. In contrast, a low smoothness constraint, as used in the IFP SGM implementation, performs more effectively on high resolution datasets since details and large disparity variations can be preserved. The reduced noise due to a greater smoothness constraint is also visible in the comparison of the two different matching costs MI and Census, since the constraint is more effective for the Census case.

Length measurement error is expressed as the distance between the estimated length on the artefact point cloud and the certified value for that distance. Since the distances between planes 1–3 and 2–4 of the cube are certified as references by the Nikon Company, the use of this reference highlights the ability of each method to solve the scale problem without using known object distances.

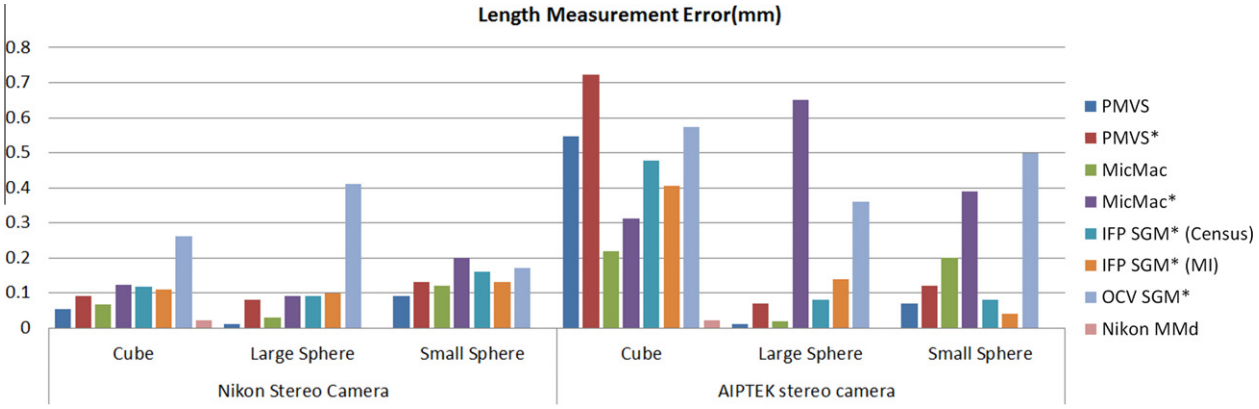

Fig. 8. Length measurement error results for both two stereo cameras.

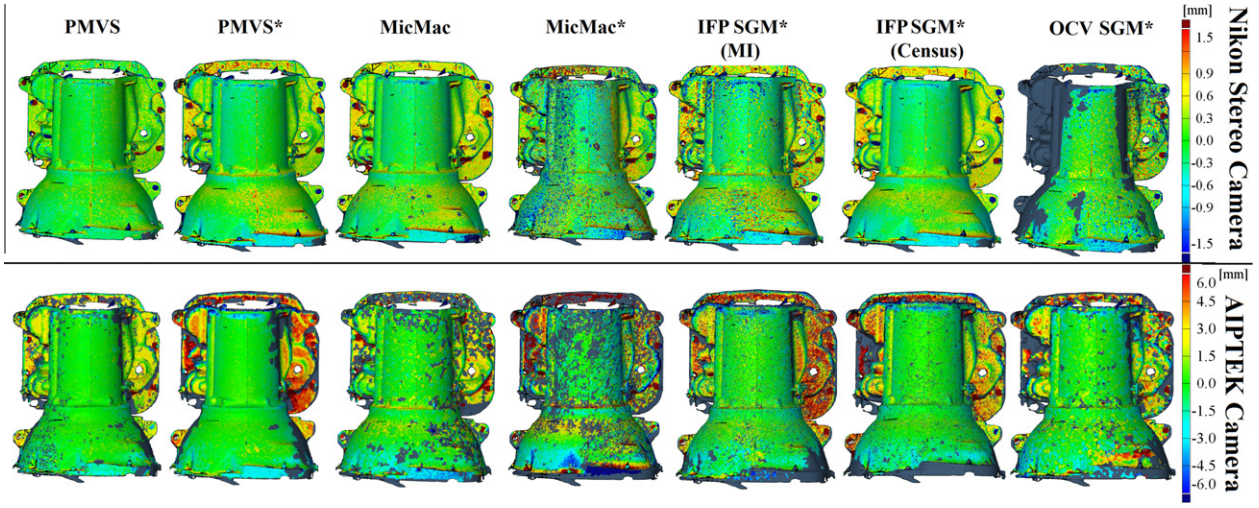

Fig. 9. Fitness errors for the data obtained with our Nikon stereo camera (top) and the AIPTEK camera (bottom).

Since the regular PMVS and MicMac solutions require known object distances to resolve the scale, the diameter of the large sphere estimated from the Nikon MMd laser scan was divided by the computed diameter for each point cloud dataset in order to compute appropriate scale factors. As a result the length measurement error of the large sphere for these solutions is almost zero (Fig. 8). Due to the shorter base and lower image quality of AIPTEK stereo camera, the length measurement errors for the point clouds obtained with this system are larger than those for our Nikon stereo camera.

In addition to the above criteria, to investigate the ability of the methods in 3D reconstruction of complex objects, another criterion (Fitness) was defined and the point clouds of the gearbox were considered for this comparison.

Fitness error is defined as the standard deviation of the surface normal length discrepancies between the estimated points on a complex object achieved with the optical measurement methods and a reference dataset. In our case the reference dataset in the form of a mesh model was generated using GOM Inspect software (v7 SR2) from the Nikon MMd scan data of the gearbox surface. The reference mesh was then compared with similarly meshed point cloud data produced with each method. In the case of the point clouds generated with regular process of PMVS and MicMac, as before, a scale factor needed to be applied to these point clouds. In this case it was computed by measuring the distance between two small reference spheres located at the top and the bottom of the gearbox.

Fig. 9 shows a visual comparison of the methods in terms of fitness error for the images captured by both camera systems from the gearbox. In this comparison, similar to the spherical errors, the Nikon laser scanner data is considered as reference data with the lowest level of error. However, the laser scanner data is not an absolute reference, so the comparisons here are relative errors. This is reinforced by the common errors apparent for the mounting holes on the rear flanges of the gearbox, caused by inaccurate scanner data. These are most clearly identifiable in the PMVS case scaled using the reference spheres (Fig. 9, top left). Nevertheless, this comparison shows the ability of the methods to produce a complete model from images captured with two stereo cameras with different imaging networks, with and without direct scaling.

With regard to comparing the methods based on model completeness, as an instance, although the OpenCV implementation of SGM produced a complete point cloud for AIPTEK images, it was unable to provide a complete point cloud for images captured with Nikon DSLR cameras. The reason for this weakness can be found in the structure of this method for merging the disparity maps. This structure directly depends on the distances between each pair of images and its next pair. These distances for Nikon DSLR imaging network are longer than AIPTEK imaging network.

This figure also proves the difference in capability between the stereo camera systems. The difference is attributable to the image quality and resolution of the respective sensors as well as differences in the exact image network configuration used. For example,

the influence of fewer images in the sides of the gearbox, as compared to the front, in AIPTEK imaging network can be seen in all of point clouds generated with these images. However, the data clearly highlights what can be achieved with relatively low cost systems. Examining the respective matching algorithm performance shows that similar fitness error patterns occur in both high and low resolution images, and sparse and dense imaging networks. Overall results demonstrate the more accurate performance of IFP SGM* (Census) and PMVS.

The comparisons also indicate residual scale errors in the data set. The directly introduced scale as proposed by the method (annotated with a*) leads to slightly degraded results compared to a later introduction of the scale in the point cloud (PMVS and MicMac without*). This is due to two specific reasons. Firstly, in the stereo camera calibration step of the presented method, the computed uncertainties of base line length were larger than expected due to the imaging configuration and this resulted in an inaccurately scaled model. Secondly, opposite to the point clouds provided with directly introduced scale, the point clouds generated with later introduction of the scale depend on the Nikon laser scan data. In a real project based on imaging, the laser scanner distances would not be available, so more attention would need to be paid to the imaging geometry to ensure an accurate scale for the model.

6. Conclusion

The paper presents a strategy which uses the base line of a stereo sensor to provide accurate 3D surface information from multi stereo images without measuring any object distances. Four independent packages for dense surface reconstruction were used to evaluate both the ability of the method to resolve the scale and assess the reliability of each package in terms of accuracy.

The results confirmed that exploiting the base lines of stereo cameras in bundle adjustment as geometric constraints can be an effective solution to overcome the problem of missing scale information in regular photogrammetric and computer vision methods. After the calibration of the stereo rig, 3D information for arbitrary scenes can be recorded efficiently since ground truth information is not required. However, between two calibrations the rigidity of the setup has to be ensured.

The results showed that the combination of a bundle adjustment with camera base constraint and dense image matching can lead to comparable accuracies to the Nikon Laser scanner if a camera of sufficient quality and an appropriate network of images are used. Within the comparison of the dense reconstruction methods, the PMVS method can lead to a scaled point cloud with more favourable accuracy than different versions of SGM and MicMac, at least in terms of flatness errors. However, the configuration of the imaging network in terms of image count, image scale and intersection angle, as well as the quality of the images, are the dominant impact factors on the resulting accuracy. In particular, high radiometric quality as present for current DSLR cameras is beneficial.

As it is proved in this work, although using a stereo camera can effectively resolve the scale, the final accuracy directly depends on the uncertainty in estimating the base line of the cameras. Therefore, the stereo camera calibration is vital in achieving improved accuracy. Using a large space with many photogrammetric targets as a calibration object, instead of a small calibration fixture, and exploiting wide-angle lenses would be an effective solution to measure the base separation more accurately. The quality and characteristics of the projected pattern is another parameter which affects the performance of the intensity matching algorithms. Regarding the amount and the location of images required, a comparison between a sparse and dense imaging networks for two stereo cameras was performed in this paper. High density networks lead to a significant increase in accuracy and point density, since the accuracy is dependent on image scale and intersection angle while the performance of dense image matching is dependent on the image similarity. Furthermore, the low performance for wide-baseline imagery and the resulting need for stereo pairs with small intersection angle can be compensated by redundancy. Thus, highly overlapping image networks are required where the image scale is chosen according to the accuracy needs.

References

Agarwal, S., Snavely, N., Simon, I., Seitz, S.M., Szeliski, R., 2009. Building Rome in a day. In: 2009 IEEE 12th International Conference, pp. 72–79.

Arya, S., Mount, D.M., Netanyahu, N.S., Silverman, R., Wu, A.Y., 1998. An optimal algorithm for approximate nearest neighbor searching fixed dimensions. Journal of the ACM 45, 891–923.

Barazzetti, L., Scaioni, M., Remondino, F., 2010. Orientation and 3D modelling from markerless terrestrial images: combining accuracy with automation. The Photogrammetric Record 25, 356–381.

Beardsley, P., Torr, P., Zisserman, A., 1996. 3D model acquisition from extended image sequences. In: Computer Vision – ECCV'96, pp. 683–695.

Birchfield, S., Tomasi, C., tul=0?>Birchfield and Tomasi. Depth discontinuities by pixel-to-pixel stereo. International Journal of Computer Vision 35, 269–293.

Brown, D.C., 1971. Close-range camera calibration. Photogrammetric Engineering 37, 855–866.

Brown, M.Z., Burschka, D., Hager, G.D., Member, S., 2003. Advances in computational stereo. IEEE Transactions on Pattern Analysis and Machine Intelligence 25, 993–1008.

Dick, A.R., Torr, P.H.S., Cipolla, R., 2004. Modelling and interpretation of architecture from several images. International Journal of Computer Vision 60, 111–134.

Ducke, B., Score, D., Reeves, J., 2010. Multiview 3D reconstruction of the archaeological site at Weymouth from image series. Computers and Graphics 35, 375–382.

Fraser, C.S., 1997. Digital camera self-calibration. ISPRS Journal of Photogrammetry and Remote Sensing 52, 149–159.

Fritsch, D., Khosravani, A.L.I.M., Cefalu, A., Wenzel, K., 2011. Multi-sensors and multiray reconstruction for digital preservation. Photogrammetrische Woche 11, 305–323.

Furukawa, Y., Ponce, J., 2009. Accurate, dense and robust Multi-View Stereopsis. IEEE Transactions on Pattern Analysis and Machine Intelligence, 1362–1376.

Furukawa, Y., Ponce, J., 2010. Accurate, dense, and robust multi-view stereopsis. IEEE Transactions on Pattern Analysis and Machine Intelligence 32, 1362–1376.

Fusiello, A., Trucco, E., Verri, A., 2000. A compact algorithm for rectification of stereo pairs. Machine Vision and Applications 12, 16–22.

Godding, R., Luhmann, T., Wendt, A., 2006. 4D Surface matching for high-speed stereo sequences. In: ISPRS Symposium Commission V, Dresden 2.2.2.

Goesele, M., Snavely, N., Curless, B., Hoppe, H., Seitz, S.M., 2007. Multi-view stereo for community photo collections. In: Proceedings, ICCV, pp. 1–8.

Granshaw, S.I., 1980. Bundle adjustment methods in engineering photogrammetry. The Photogrammetric Record 10, 181–207.

Grussenmeyer, P., Fares, S., Hullo, J.F., 2009. Photogrammetry and dense stereo matching approach applied to the documentation of the cultural heritage site of Kilwa (Saudi Arabia). In: XXII CIPA, Symposium, pp. 1–6.

Hao, X., Mayer, H., 2003. Orientation and auto-calibration of image triplets and sequences. International Archives of Photogrammetry Remote Sensing and Spatial Information Sciences 34, 73–78.

Hartley, R., Zisserman, A., 2004. Multiple View Geometry in Computer Vision, second ed. Cambridge University Press.

He, G., Novak, K., Feng, W., 1993. On the integrated calibration of a digital stereo-vision system. International Archives of Photogrammetry and Remote Sensing 29, 139.

Hirschmüller, H., 2005. Accurate and efficient stereo processing by semi-global matching and mututal information. In: IEEE Conference for Computer Vision and Pattern Recognition, vol. 2. San Diego, CA, USA, pp. 807–814.

Hirschmuller, H., 2008. Stereo processing by semiglobal matching and mutual information. IEEE Transactions on Pattern Analysis and Machine Intelligence 30, 328–341.

Hirschmüller, H., Scharstein, D., 2007. Evaluation of cost functions for stereo matching. In: IEEE Conference on Computer Vision and Pattern Recognition, CVPR '07, pp. 1–8.

King, B., 1995. Bundle adjustment of constrained stereopairs – mathematical models. Geomatics Research Australasia, 67–92.

Läbe, T., Förstner, W., 2006. Automatic relative orientation of images. In: Proceedings of the 5th Turkish–German Joint Geodetic Days 3.

Lowe, D.G., 1999. Object recognition from local scale-invariant features. In: The Proceedings of the Seventh IEEE International Conference on Computer Vision, pp. 1150–1157.

Merrell, P., Akbarzadeh, A., Wang, L., Mordohai, P., Frahm, J.M., Yang, R., Nistér, D., Pollefeys, M., 2007. Real-time visibility-based fusion of depth maps. In: Computer Vision, ICCV 2007. IEEE 11th International Conference, pp. 1–8.

Nister, D., 2004. Automatic passive recovery of 3D from images and video. In: 2nd International Symposium on 3D Data Processing, Visualization and Transmission, 3DPVT 2004. Proceedings, pp. 438–445.

Olague, G., Dunn, E., 2007. Development of a practical photogrammetric network design using evolutionary computing. The Photogrammetric Record 22, 22–38.
Pierrot-Deseilligny, M., Deluca, L., Remondino, F., 2011. Automated image-based procedures for accurate artifacts 3D modeling and orthoimage generation. Geoinformatics FCE CTU Journal 6, 291–299.
Pierrot-Deseilligny, M., Paparoditis, N., 2006. A multiresolution and optimization-based image matching approach: an application to surface reconstruction from SPOT5-HRS stereo imagery. International Archives of Photogrammetry, Remote Sensing and Spatial Information Sciences 36, 41.
Pollefeys, M., Koch, R., Gool, L.V., 1999. Self-calibration and metric reconstruction inspite of varying and unknown intrinsic camera parameters. International Journal of Computer Vision 32, 7–25.
Remondino, F., El-Hakim, S., 2006. Image-based 3D modelling: a review. The Photogrammetric Record 21, 269–291.
Remondino, F., Ressl, C., 2006. Overview and experiences in automated markerless image orientation. International Archives of Photogrammetry, Remote Sensing and Spatial Information Sciences 36, 248–254.
Remondino, F., Zhang, L., 2006. Surface reconstruction algorithms for detailed close-range object modeling. IAPRSSIS 36, 117–121.
Roncella, R., Forlani, G., Remondino, F., 2005. Photogrammetry for geological applications: automatic retrieval of discontinuity orientation in rock slopes. In: Videometrics IX, Electronic Imaging, IS&T/SPIE 17th Annual, Symposium, pp. 17–27.
Seitz, S.M., Curless, B., Diebel, J., Scharstein, D., Szeliski, R., 2006. A comparison and evaluation of multi-view stereo reconstruction algorithms. In: Computer Vision and Pattern Recognition, 2006 IEEE Computer Society, 1, pp. 519–528.
Shortis, M.R., Harvey, E.S., 1998. Design and calibration of an underwater stereo-video system for the monitoring of marine fauna populations. International Archives of Photogrammetry and Remote Sensing 32, 792–799.
VDI/VDE 2634/Part2, 2002. Optical 3-D Measuring Systems – Optical Systems based on Area Scanning.
VDI/VDE 2634/Part3, 2008. Optical 3-D Measuring Systems – Multiple View Systems based on Area Scanning.
Viola, P., Wells, W.M., I., 1995. Alignment by Maximization of Mutual Information. In: Computer Vision, 1995. Proceedings, pp. 16–23.
Wenzel, K., Abdel-Wahab, M., Fritsch, D., 2011. Multi-camera System for Close Range Point Cloud Acquisition. LC3D workshop.
Xiao, Z., Liang, J., Yu, D., Tang, Z., Asundi, A., 2010. An accurate stereo vision system using cross-shaped target self-calibration method based on photogrammetry. Optics and Lasers in Engineering 48, 1252–1261.
Yang, B., Li, H., Zhang, R., Dong, L., 2011. A sequential algorithm for digital camera calibration with single images, In: International Conference on Asia Agriculture and Animal IPCBEE. IACSIT Press, Singapoore, 13.
Zabih, R., Woodfill, J., 1994. Non-parametric local transforms for computing visual correspondence. In: Eklundh, J.-O. (Ed.), Computer Vision—ECCV '94. Lecture Notes in Computer Science. Springer Berlin/Heidelberg, pp. 151–158.
Zach, C., 2008. Fast and high quality fusion of depth maps. In: Proceedings of the International Symposium on 3D Data Processing, Visualization and Transmission (3DPVT), p. 1.

Websites:

123D Catch, 2012. Autodesk 123D Catch. <http://labs.autodesk.com/utilities/photo_scene_editor/> (accessed 23.11.12).
Agisoft, 2012. Agisoft PhotoScan. <www.agisoft.ru/> (accessed 23.11.12).
Bundler, 2010. Structure From Motion method for Unordered Image Collections. <http://phototour.cs.washington.edu/bundler/> (accessed 23.11.12).
CMVS, 2011. Clustering Views for Multi-View Stereo. <http://grail.cs.washington.edu/software/cmvs/> (accessed 23.11.12).
Insight3D, 2007. Open source image based 3D modelling software. <http://insight3d.sourceforge.net/> (accessed 23.11.12).
iWitness and Australis, 2012. SOlution for Large Volume Enhanced Metrology (Solve). <www.solve3d.net/ENG/iWeproducts.htm> (accessed 23.11.12).
OpenCV SGM, 2011. Camera Calibration and 3D Reconstruction. <http://opencv.willowgarage.com/documentation/cpp/camera_calibration_and_3d_reconstruction.html> (accessed 23.11.12).
Photomodeler Scanner, 2012. Photomodeler. <www.photomodeler.com/products/pm-scanner.htm> (accessed 23.11.12).
Photosynth, 2012. Microsoft Photosynth. <http://photosynth.net/> (accessed 23.11.12).
PMVS Version 2, 2010. Patch-based Multi-View Stereo. <http://grail.cs.washington.edu/software/pmvs/> (accessed 23.11.2012).
Shape Capture, 2012. ShpaeQuest Inc. <http://www.shapecapture.com/home.html> (accessed 23.11.12).
VMS, 2012. Geometric Software. <www.geomsoft.com> (accessed 23.11.12).
MicMac, Tapiaco and Apero, 2007. Tools and Acquisition Protocols for Enhancing Artifacts Documentation. <http://www.tapenade.gamsau.archi.fr/TAPEnADe/Tools.html> (accessed 23.11.12).